



Cite this: *Chem. Commun.*, 2021, 57, 6608

Received 12th April 2021,
Accepted 27th May 2021

DOI: 10.1039/d1cc01940f

rsc.li/chemcomm

Construction of a novel asymmetric imidazole-cored AIE probe for ratiometric imaging of endogenous leucine aminopeptidase†

Xueyan Huang,^{id} ^{ab} Qian Lei,^{ab} Shuai Huang,^{ab} Hongliang Zeng,^c Bin Feng,^{ab} Qinghai Zeng,^d Yibo Hu^d and Wenbin Zeng^{id} ^{*ab}

We report a rational strategy to deliberately construct the first asymmetric tetraarylimidazole-based AIE probe, integrating AIE behavior in synergy with ESIPT character to image endogenous LAP for the first time. It offered good sensitivity and selectivity, and concomitantly, was applied successfully for real-time tracking of LAP in the cisplatin-induced liver injury zebrafish model.

Leucine aminopeptidase (LAP), one of the most important exopeptidases, can selectively release leucine residues from the N-terminus of protein or peptide substrates and plays a vital role in numerous physiological and pathological processes.^{1,2} The abnormal catalytic function of LAP often causes disorder of peptide activation, tumour cell proliferation, intrinsic resistance toward drug, invasion and angiogenesis.^{3,4} Increased LAP expression nearly correlates with many diseases, such as hepatic dysfunction or liver cancer, therefore enabling it to serve as a potential biomarker for cancer diagnosis.^{5,6}

The invention of the light microscope has thoroughly accelerated the great cause of uncovering the microbial world.⁷ For the on-site dynamic monitoring of LAP, a fluorescence probe is regarded as a preferential strategy due to its excellent spatial-temporal resolution, non-invasiveness and high specificity.⁸ Unfortunately, existing probes often suffer from insufficient anti-interference ability thereby producing false-negative or false-positive signals,⁹ and in addition some probes also have strong background fluorescence or quenched fluorescence at high concentration in an aqueous environment, which greatly limits their application in

living cells. This prompted us to develop novel LAP probes with a self-calibration effect and robust fluorescence emission.

Aggregation-induced emission (AIE) materials, different from traditional dyes, exhibit intensive fluorescence upon aggregation with strong resistance toward photobleaching. Furthermore, AIE fluorophores also possess flexible controllability, high sensitivity and high selectivity, making them ideal candidates for enzyme detection.^{10,11} Prior to this, the implementation of the AIE strategy in LAP detection was scarcely reported.¹² Among the extensive fluorescent scaffolds, tetraarylimidazole is a typical building block of AIE, and related imidazole derivatives have been employed successfully in the detection of various biomolecules in living systems.^{13,14} These AIE fluorophores based on tetraarylimidazole were synthesized by the one-pot method,¹⁵ in which the major structural feature is the two identical aryl substituents at the 4,5-positions of imidazole, largely limiting their capability for derivation (Scheme 1A). Therefore, efforts to construct these fluorophores with asymmetric substituents at the 4,5-positions become ground breaking in developing of novel AIE fluorophores, and in the meanwhile, would spark more multi-functional fluorescent probes.

Herein, we put forward an alternative method to construct imidazole fluorophores with various aryl groups at 4,5-positions (Scheme 1B) and further successfully developed a novel AIE fluorescent probe **ASSI-Leu** for tracking endogenous LAP. The probe was designed to purposefully incorporate the classic 2-(2'-hydroxyphenyl) benzothiazole (HBT) skeleton into the 5-position aromatic

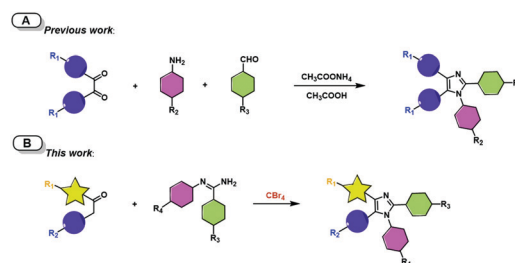
^a Xiangya School of Pharmaceutical Sciences, Central South University, Changsha, 410013, P. R. China. E-mail: wbzeng@hotmail.com, wbzeng@csu.edu.cn; Fax: +86-731-82650459; Tel: +86-731-82650459

^b Hunan Key Laboratory of Diagnostic and Therapeutic Drug Research for Chronic Diseases, Changsha 410078, China

^c Hunan Academic of Chinese Medicine, Inst Chinese Mat Med, Changsha, P. R. China

^d Dermatological Department, 3rd Xiangya Hospital, Central South University, Changsha, 410078, P. R. China

† Electronic supplementary information (ESI) available. See DOI: 10.1039/d1cc01940f

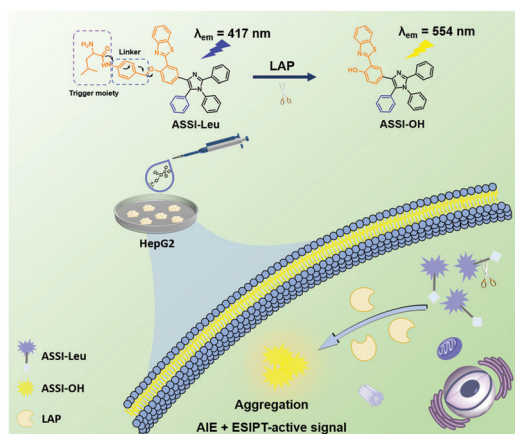


Scheme 1 Strategies for the construction of tetraarylimidazole-based AIE fluorophores.

ring to avail both AIE and excited-state intramolecular proton transfer (ESIPT) characters. Then the hydrogen bond donor was elaborately blocked by a LAP substrate *L*-leucine amide which would prevent the ESIPT process, thus, only enol emission can be observed.¹⁶ However, upon exposure toward LAP, the block unit Leu is cleaved from the fluorophore, accompanied by the fluorescence signal, which is ascribed to the combined AIE characteristics and keto-emission behaviour. The relative change of the two individual emissions could eliminate the interference of external environment factors, thereby affording **ASSI-Leu** as an efficient tool for *in situ* ratiometric imaging of endogenous LAP (Scheme 2). This strategy bestows the advantages of large Stokes' shift, high sensitivity and selectivity, favorable photostability and low cytotoxicity on the novel probe. Benefiting from these advantages, the real-time tracking of LAP activity in hepatoma cells and zebrafish models was achieved.

We employed ketone substrates and amidine derivatives as raw materials by referring to Zhou's contribution to the CBr₄-based synthesis.¹⁷ In the carbon tetrabromide-mediated tandem cyclization, an imidazole derivative with asymmetrically substituted aryl groups at 4,5-positions of the imidazole ring was easily synthesized. HBT was incorporated into the 5-position of the imidazole ring to obtain the chromophore with both AIE and ESIPT properties. The detailed synthetic routes of **ASSI-Leu** are described in Scheme S1 (ESI[†]).

Initially, we investigated the photophysical properties of **ASSI-OH** in various solvents. The UV/Vis spectra exhibited the absorption maximum at 365 nm, and there was no obvious keto-emission in the fluorescence spectra (Fig. S1, ESI[†]), which did not seem to tally with the optical characteristics of the traditional ESIPT dyes. To gain further insights into this photophysical behavior, we performed the TD/DFT calculations at the PBE0/def2-SVP level to optimize enol geometry and adopted the method of constructing a potential energy surface (PES) to explore the ability of **ASSI-OH** to experience the ESIPT process. A single point calculation along the relaxed S₁ paths yielded the unrelaxed S₀ energy profiles. As shown in Fig. 1A, there was an energy barrier of 0.638 kcal mol⁻¹ in the S₁ state for the conversion of enol into keto species, suggesting the low efficiency of the IPT reaction.



Scheme 2 Schematic illustration of probe **ASSI-Leu** for detecting LAP and the performance in living cells.

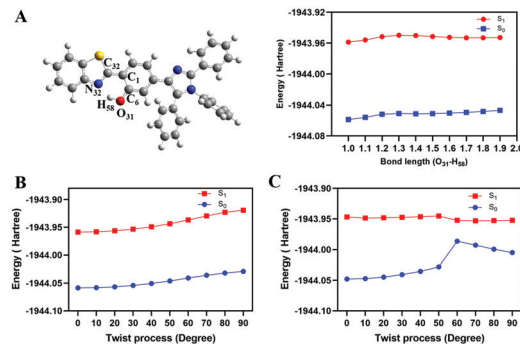


Fig. 1 Related theoretical calculations of compound **ASSI-OH**. (A) Optimized enol minimum-energy structure in the S₁ state and the constructed potential energy scan surface of both S₀ and S₁ states of **ASSI-OH** as a function of O₃₁-H₅₈. The PESs' illustration of enol form (B) and keto form (C) as a function of dihedral angle C₆-C₁-C₃₀-N₃₂.

Thus, **ASSI-OH** mainly existed in the enol form in an excited state. Subsequently, a better understanding could be derived from the PES of twisted intramolecular charge transfer (TICT). The calculated result showed that the twisting process of the enol form of **ASSI-OH** was obstructed, and the TICT process could not occur and appeared as a luminous local excited state (Fig. 1B). However, for the keto form, the TICT dark state dominated in governing the luminescence behavior due to the lower energy of the TICT state (Fig. 1C), which helps in explaining the phenomenon that only emission of the enol form was observed during the solvent effect investigation.

Then, we studied the AIE characteristics of **ASSI-OH** in the DMSO/water mixture with different water fractions (*f_w*). In pure DMSO solution, it showed blue fluorescence which was assigned to enol emission. With an increase in the water percentage to 60%, the fluorescence intensity had a remarkable enhancement at 554 nm (Fig. S2, ESI[†]), evidently suggesting that **ASSI-OH** was AIE-active. This phenomenon could be ascribed to that the intramolecular rotation and vibration were restricted in the aggregation state; meanwhile, the intramolecular hydrogen bonds were easy to form, thereby reducing the barrier of enol-keto conversion to the active ESIPT process. As the *f_w* was above 60%, the reduction in the fluorescence could be explained by the fact that those aggregates reached a critical point and precipitated out from the solution with weaker emission. Combined with the above solvation behavior, this novel asymmetrically substituted imidazole-based fluorophore exhibited unique properties. Concretely, it showed AIE performance at the keto emission location in the aggregation state due to the restraint of the TICT and activated ESIPT processes, while only enol emission was observed in the solution owing to the high energy barrier. This aggregation-assisted ESIPT process and the behavior of showing AIE properties at the position of keto emission are synchronous and consistent.

Subsequently, the optical responses of **ASSI-Leu** toward LAP in an aqueous solution containing 10% DMSO at 37 °C were systematically investigated. After incubation with LAP, the absorbance of **ASSI-Leu** sharply enhanced (Fig. S3, ESI[†]). And as anticipated, a significant ratiometric fluorescence signal (*I*_{554 nm}/*I*_{417 nm}) was observed in the titration experiment of the enzymatic reaction (Fig. 2A). With the increase of LAP concentration, the fluorescence

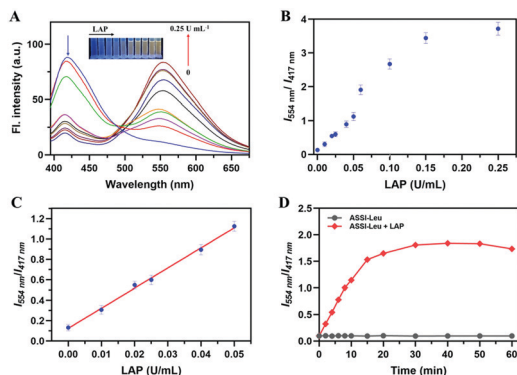


Fig. 2 (A) Emission spectra of **ASSI-Leu** (5 μM) after 40 min upon treatment with increasing concentrations of LAP (0–0.25 U mL^{-1}) in aqueous solution (10% DMSO, v/v) at 37 $^{\circ}\text{C}$. (B) Plots of fluorescence ratio ($I_{554\text{nm}}/I_{417\text{nm}}$) versus LAP concentration. (C) Linear fitting curve of fluorescence ratio ($I_{554\text{nm}}/I_{417\text{nm}}$) toward the concentration of LAP from 0–0.05 U mL^{-1} . (D) Time dependence of $I_{554\text{nm}}/I_{417\text{nm}}$ for **ASSI-Leu** in the presence (red) and absence (gray) of LAP. $\lambda_{\text{ex}} = 365\text{ nm}$.

intensity at 417 nm decreased progressively, and a red-shifted fluorescence peak at 554 nm emerged concurrently, which corresponded to the evolution of **ASSI-OH**. Moreover, the fluorescence intensity at 554 nm demonstrated more than a 7-fold increase upon reaction with 0.1 U mL^{-1} LAP for 1 h. However, this obvious fluorescence enhancement could be suppressed in the presence of the LAP inhibitor bestatin, substantiating that the signal is generated by LAP catalysis in a specific manner (Fig. S4, ESI †). In addition, the fluorescence signal ratio ($I_{554\text{nm}}/I_{417\text{nm}}$) was observed to increase gradually, presenting evident concentration dependence (Fig. 2B). Notably, it exhibited good linearity with LAP in 0–0.05 U mL^{-1} ($R^2 = 0.997$) and the detection limit was determined to be $2.983 \times 10^{-3} \text{ U mL}^{-1}$, indicative of high sensitivity (Fig. 2C). Hence, the curve was promising to provide convenience for LAP detection.

Concurrently, time-dependent fluorescence measurement was carried out for exploring the kinetics of the hydrolysis reaction by LAP. A concomitant ratiometric fluorescence signal increase was observed in the initial stage and took about 40 min to reach the plateau, while the signal without LAP remained unchanged (Fig. 2D and Fig. S5, ESI †). Clearly, it implicated the potential of **ASSI-Leu** for fast and effective detection of LAP. Then, the selectivity experiment was conducted by incubating the probe with a series of important biomolecules. As illustrated in Fig. S6 (ESI †), none of these species could trigger the change of the ratiometric fluorescence signal, indicating the satisfactory specificity to LAP over all other interferents, which is valuable in biological applications. Next, we investigated the pH effect on the probe. The fluorescence signal of the probe itself remained consistently unchanged in the test range, while the reaction system could achieve the maximum fluorescence ratio enhancement in neutral media, indicating that **ASSI-Leu** can be used for the superior detection of LAP under physiological conditions (Fig. S7, ESI †).

To confirm the activation effect of LAP on **ASSI-Leu**, we injected the mixture upon incubation with LAP to an electron spray ionization-mass spectrometer (ESI-MS). As shown in Fig. S8 (ESI †), the peaks of m/z 740.29 ($[\text{M}-\text{H}]^+$) were quite weak,

while the peak of m/z 522.15 ($[\text{M}-\text{H}]^+$) corresponding to **ASSI-OH** dominantly appeared. This unequivocally supported the LAP-triggered cleavage of the probe causing the release of the free fluorophore. Also, according to the distance-dependent photonic properties of the fluorophore, dynamic light scattering (DLS) was performed, and the results manifested the formation of nanoparticles with an average size of 200 nm after incubation with LAP at 37 $^{\circ}\text{C}$ for 30 min (Fig. S9, ESI †). These results confirmed the cleavage of **ASSI-Leu** by LAP and the aggregation of the released **ASSI-OH**. Moreover, these were further indicated by inhibitor experiments (Fig. S4, ESI †).

From the above observations, **ASSI-Leu** exhibited good specificity and sensitivity for LAP in aqueous solution and therefore is expected to realize the ratiometric imaging of endogenous LAP. First, HepG2 cells (a human hepatoma cell line with overexpressed LAP) were selected to evaluate the biocompatibility *via* cell viability assay. The results showed that the cells retained high cell viability upon 24 h incubation with various concentrations of the probe (2.5–40 μM) (Fig. S10, ESI †), indicating the negligible cytotoxicity of **ASSI-Leu**. Next, the potential to detect endogenous LAP was investigated in HepG2 cells. After being treated with **ASSI-Leu** for 30 min, bright yellow fluorescence could be captured in the 490–560 nm emission channel upon excitation at 405 nm (Fig. S11, ESI †). This benefited from the aggregation of released **ASSI-OH** by the enzymatic transformation in living cells, which allows *in situ* LAP imaging due to the synergistic effect of AIE and the activated ESIPT process. Notably, the fluorescence signal increased in a dose-dependent manner. Then, the time-course assay was conducted to study the real-time ratiometric imaging ability. As illustrated in Fig. 3, when incubated with **ASSI-Leu** for 10 min, channel one gave strong blue fluorescence (410 nm–470 nm) while channel two showed weak yellow fluorescence. The measured fluorescence ratio from channel two to channel one was about 0.79. With the prolongation of incubation, the fluorescence intensity of channel one gradually decreased accompanied by a remarkable fluorescence enhancement in channel two, and the ratio improved to be 2.47 after 1 h of incubation.

Subsequently, HepG2 cells were exposed to bestatin for 1 hour and then treated with **ASSI-Leu** for another 30 min; the fluorescence intensity in channel two was significantly suppressed and the fluorescence ratio decreased to 0.72 (Fig. S12, ESI †). The above results undeniably demonstrated the ability of the probe to real-time track endogenous LAP, which granted it the potential for clinicopathological analysis. Notably, it was found that the fluorescence signal was mainly located at a certain site rather than being evenly distributed, which prompted us to further carry out a subcellular colocalization study. As shown in Fig. S13 (ESI †), there was a substantial overlap between the yellow fluorescence of the probe and the red fluorescence of LysoTracker red. The change of emission intensity in the linear region of interest (ROI) exhibited a synchronous trend, and the Pearson's correlation coefficient was 0.67 (Fig. S14 and S15 ESI †). This result suggested that the probe may mainly accumulate in lysosomes.

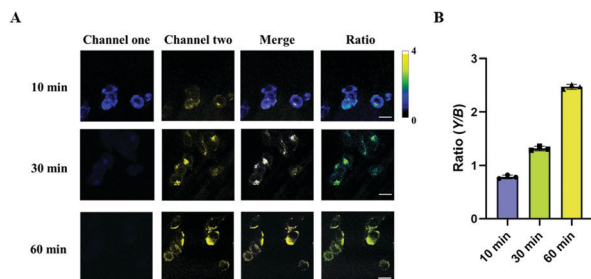


Fig. 3 (A) Confocal fluorescence images of HepG2 cells incubated with **ASSI-Leu** (10 μM) for 10 min, 30 min and 60 min. Channel one was collected from 410 nm to 470 nm (blue); channel two was collected from 490 nm to 560 nm (yellow), $\lambda_{\text{ex}} = 405$ nm. The images of the ratio were generated with ImageJ software. (B) The relative fluorescence intensity ratio from channel one to channel two (Y/B). Data represent the mean standard error ($n = 3$). Scale bar is 10 μm .

Encouraged by the above results, we further employed the zebrafish model to validate the feasibility of **ASSI-Leu** to image LAP *in vivo*. It was documented that the LAP level is significantly associated with the drug induced damage in the case of overdose cisplatin treatment.¹⁸ To strengthen this matter, 7 day old zebrafish were pre-treated with 0.1 $\mu\text{g mL}^{-1}$ cisplatin for 12 h, and then loaded with the probe for confocal imaging. The results clearly showed a strongly emerged yellow signal in channel two as time prolongs and the synchronous attenuation of the blue signal in channel one (Fig. 4A–C), which exhibited a high signal-to-noise ratio. Fig. 4E illustrates the change of fluorescence ratio between channel two and channel one. After incubation for 1 h, the ratio increased to 3.15. Similar to previous results in living cells, the fluorescence ratio significantly diminished in the presence of inhibitor bestatin, further validating the role of LAP in the change of fluorescence (Fig. 4D). Taken together, we can reasonably conclude that **ASSI-Leu** possessed high selectivity for the specific tracking of LAP in living organisms, thereby holding the potential for biomedical applications.

In summary, we developed the first tetraarylimidazole-based AIE fluorophore with different aryl substituents at 4,5-positions

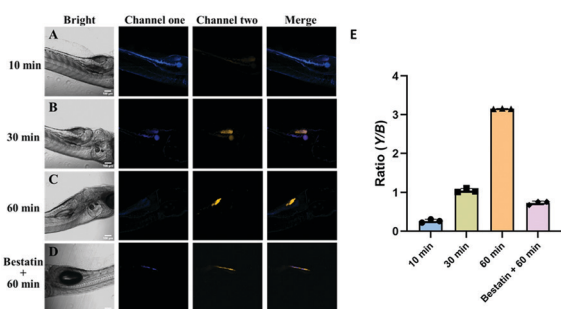


Fig. 4 Confocal fluorescence images for visualizing endogenous LAP in the cisplatin-induced zebrafish acute liver injury model using **ASSI-Leu**. The zebrafish models were pretreated with 0.1 $\mu\text{g mL}^{-1}$ cisplatin and then incubated with **ASSI-Leu** (10 μM) for 10 min (A), 30 min (B) and 60 min (C), respectively. (D) The pretreated zebrafish models were incubated with bestatin (100 μM) for 12 h and then cultured with **ASSI-Leu** (10 μM). (E) Fluorescence ratios (Y/B) of the corresponding fluorescence images. Channel one: 410–470 nm; channel two: 490–560 nm, $\lambda_{\text{ex}} = 405$ nm. Data represent the mean standard error ($n = 3$). Scale bar is 100 μm .

by employing an alternative synthesis strategy. Owing to the incorporation of the HBT skeleton, the fluorophore exhibited AIE-assisted ESIPT behaviour, and its unique optical properties were rationalized in detail by theoretical analysis. To the best of our knowledge, the obtained probe **ASSI-Leu** is the first implementation of combining the AIE mechanism with ESIPT character in ratiometric tracking of LAP accurately. The probe offered large Stokes' shift, appreciable biocompatibility, and high sensitivity and selectivity. Remarkably, it has been successfully used in hepatoma cells and drug-induced liver injury zebrafish models, indicating the potential for facilitating diagnosis in complex biosystems. It is worth mentioning that the novel building block **ASSI-OH** and its synthesis strategy are anticipated to stimulate more fluorescent probes bearing multi-functional sites as the potential biological vehicle. Related studies are being progressively carried out as well in our laboratory.

The authors gratefully acknowledge the financial support from the National Natural Science Foundation of China (81971678 and 81671756), the Science and Technology Foundation of Hunan Province (2020SK3019, 2019SK2211 and 2019GK5012), and the Research Innovation Fund for Postgraduates of Central South University (2018zzts877).

Conflicts of interest

There are no conflicts to declare.

Notes and references

- M. Tsujimoto, Y. Goto, M. Maruyama and A. Hattori, *Heart Failure Rev.*, 2008, **13**, 285–291.
- M. Matsui, J. H. Fowler and L. L. J. Walling, *Biol. Chem.*, 2006, **387**, 1535–1544.
- S. K. Burlley, P. R. David and W. N. Lipscomb, *Proc. Natl. Acad. Sci. U. S. A.*, 1991, **88**, 6916–6920.
- A. Taylor, *FASEB J.*, 1993, **7**, 290–398.
- T. Yamazaki, T. Akada, O. Niizeki, T. Suzuki and H. Miyashita, *Blood*, 2004, **104**, 2345–2352.
- J. J. Reichling and M. M. Kaplan, *Dig. Dis. Sci.*, 1988, **33**, 1601–1614.
- A. J. Wollman, R. Nudd, E. G. Hedlund and M. C. Leake, *Open Biol.*, 2015, **5**, 150019.
- H. Huang, H. Tanaka, B. D. Hammock and C. Morisseau, *Anal. Biochem.*, 2009, **391**, 11–16.
- W. Xu, C. L. Teoh, J. Peng, D. Su, L. Yuan and Y. T. Chang, *Biomaterials*, 2015, **56**, 1–9.
- J. Mei, N. L. Leung, R. T. Kwok, J. W. Lam and B. Z. Tang, *Chem. Rev.*, 2015, **115**, 11718–11940.
- G. Feng and B. Liu, *Acc. Chem. Res.*, 2018, **51**, 1404–1414.
- S. L. Huang, Y. L. Wu, F. Zeng, J. J. Chen and S. Z. Wu., *Anal. Chim. Acta*, 2018, **1031**, 169–177.
- T. Gao, S. Wang, W. Lv, M. Liu, H. Zeng, Z. Chen, J. Dong, Z. Wu, X. Feng and W. Zeng, *Chem. Commun.*, 2018, **54**, 3578–3581.
- T. Gao, H. Zeng, H. Xu, F. Gao, W. Li, S. W. Zhang, Y. Liu, G. Luo, M. D. Li, D. Jiang, Z. Chen, Y. Wu, W. Wang and W. Zeng, *Theranostics*, 2018, 1911–1922.
- T. Gao, S. Yang, X. Z. Cao, J. Dong, N. Zhao, P. Ge, W. Zeng and Z. Cheng, *Anal. Chem.*, 2017, **89**, 10085–10093.
- A. C. Sedgwick, L. L. Wu, H. H. Han, S. D. Bull, X. P. He, T. D. James, J. L. Sessler, B. Z. Tang, H. Tian and J. Y. Yoon, *Chem. Soc. Rev.*, 2018, **47**, 8842–8880.
- X. Q. Zhou, H. J. Ma, C. Shi, Y. X. Zhang, X. X. Liu and G. S. Huang, *Eur. J. Org. Chem.*, 2017, 237–240.
- Q. Y. Gong, W. Shi, L. H. Li and H. M. Ma, *Chem. Sci.*, 2016, **7**, 788–792.